Int. J. Heat Mass Transfer. Vol. 36, No. 3, pp. 793–807, 1993
Printed in Great Britain

0017–9310/93 $6.00 + 0.00

Double-diffusive fingering convection in a porous medium

FALIN CHEN
Institute of Applied Mechanics, National Taiwan University, Taipei, Taiwan 10764, R.O.C.

and

C. F. CHEN
Department of Aerospace and Mechanical Engineering, University of Arizona, Tucson, AZ 85721, U.S.A.

(*Received* 12 *August* 1991 *and in final form* 22 *November* 1991)

Abstract—We consider nonlinear two-dimensional, horizontally periodic, double-diffusive fingering convection in a saturated porous medium. The Darcy equation, including Brinkman and Forchheimer terms to account for viscous and inertia effects, respectively, is used for the momentum equation. A mixed Galerkin–finite difference method (Galerkin in the horizontal direction, finite difference in the vertical direction) is developed to solve the initial boundary value problem. Different values of the stabilizing temperature gradient, characterized by a thermal Rayleigh number R_T, ranging between 1 and 50 are considered. The stability boundaries which separate regions of different type of convective motion are identified in terms of R_T and R_S, the solute Rayleigh number. For $R_T = 1$, for instance, the steady convective flow which bifurcates from the motionless conduction solution at $R_S^1 = 4\pi^2 + 1$ persists in the face of small disturbances up to at least $R_S = 10R_S^1$. At approximately $R_S^2 = 440$, a transition to time-periodic convection occurs. For a larger stabilizing temperature gradient ($R_T = 50$), the steady-convective motion is stable with respect to small disturbances for $R_S^1 = 4\pi^2 + 50 < R_S < 4R_S^1$. At approximately $R_S^2 = 405$, a periodic convection occurs and persists up to $R_S^3 = 440$, at which a multipeaked periodic solution is found.

1. INTRODUCTION

THE DOUBLE-DIFFUSIVE fingering convection is found to be important in the vertical transport of the salt in the ocean [1]. While in the porous medium, although not yet observed in nature, the vertical contaminant transport in groundwater due to buoyancy-driven motions may play a significant role in many situations. In the directional solidification of a binary alloy when cooling from below, for another example, there is a dendritic region separating the melt from the pure solid region [2]. In the dendritic region, which used to be recognized as a porous mushy zone, there are gradients of temperature and concentration existing simultaneously; which may be conducive to the occurrence of the fingering convection [3].

The double-diffusive convection, according to its dynamic characteristics, can be categorized into 'fingering' and 'diffusive' configurations. To make doubly-diffusive convection possible, the fluid must contain at least two components with different molecular diffusivities. In the fingering convection regime, the faster diffusing component is stabilizing and the slower diffusing component destabilizing to the vertical density gradient; and vice versa for diffusive convection.

A nonlinear treatment of double-diffusive fingering convection in a fluid layer was first presented by Straus [4]. He found that only small-scale motions are stable and the wavelength of the preferred mode compares favorably with the wavelength that maximizes the salt flux. Piacsek and Toomre [5] studied the finite amplitude growth of salt fingers across the interface in a two-layer fluid (warm saline over cold fresh water). Their study emphasized evolving shapes of the fingers, their collective growth behavior, and the associated vertical fluxes of heat and salt. They found that the fingers terminate as they penetrate into the quiescent fluid region and their shapes become bulbous. Because of the dynamic feature of the flow instability, the double-diffusive problem with saltier and warmer fluid below (diffusive convection) has attracted relatively much more attention than fingering convection has in the last decade. For example, Huppert and Moore [6] employed perturbation analysis and direct numerical simulation of the governing equations to trace out the possible forms of large-amplitude motion as a function of the Rayleigh number, Prandtl number, and Lewis number. They found two branches of time-dependent asymptotic solutions, which bifurcate from the motionless conduction solution. One is an oscillatory branch emanating from the linear oscillatory mode. The other branch is the one of steady solutions, and emanates from the linear monotonic mode. Knobloch *et al.* [7] uncovered a range of temporal chaos in which sequences of period-doubling bifurcations follow the periodic oscillations found by Huppert and Moore. Murray [8], in his disser-

NOMENCLATURE

B	form drag constant, equation (8)
C	coefficient of Adams–Bashforth scheme
C_p	specific heat of fluid
d	diameter of glass beads which constitute the porous medium
D	differential operator, d/dz
Da	Darcy number, K/h^2
F	nonlinear functional, equations (25)–(28)
g	gravitational acceleration constant
G	$(\rho_r C_p)_m/(\rho_r C_p)_f$
h	depth of the porous medium
k	unit vector in z-direction
I	convolution product, equations (29) and (30)
K	permeability, equation (6)
Le	Lewis number, κ_S/κ_T
Nu	Nusselt number, equation (32)
P	pressure
Pr	Prandtl number, ν/κ_T
Q	coefficient of Fourier decomposition of $\|\mathbf{u}\|$
R_T	thermal Rayleigh number, $g\gamma(T_h-T_l)hK/(\nu\kappa_T)$
R_S	solute Rayleigh number, $g\beta(S_h-S_l)hK/(\nu\kappa_S)$
S	salinity
Sc	Schmidt number, ν/κ_S
Sh	Sherwood number, dS_0/dz at $z = 1$
t	time
T	temperature
u	velocity vector, (v, w)
v	horizontal velocity
V	horizontal velocity in Fourier decomposition
w	vertical velocity
W	vertical velocity in Fourier decomposition.

Greek symbols

α	nondimensional wavenumber
β	solute expansion coefficient, equation (5)
γ	thermal expansion coefficient, equation (5)
κ_f	thermal diffusivity of fluid
κ_g	thermal diffusivity of glass bead
κ_S	solute diffusivity of species in porous medium
κ_T	thermal diffusivity of porous medium
μ	dynamic viscosity
ν	kinematic viscosity
ρ	density of fluid
ϕ	porosity.

Subscripts

h	lower boundary
k	index of Fourier decomposition
l	upper boundary
r	reference property
0	basic state.

Superscripts

1	first bifurcation from quiescent state to steady state
2	second bifurcation from steady state to periodic state
3	third bifurcation from periodic state to arbitrarily unsteady state.

tation, investigated double-diffusive convection in a horizontal porous layer bounded by two rigid planar boundaries at the top and bottom, by both experimental and numerical approaches. He found that the oscillatory motion predicted by linear theory was unstable at finite amplitude. The breakdown of the initial oscillatory motion is followed by a large increase in the heat transport, as observed in his experiments (see also Murray and Chen [9]).

In the experimental works, Griffiths [10] performed a double-diffusive convection in a porous medium by using both a Hele–Shaw cell and a sand tank model to study the diffusive configuration. His results were suitable to explain some of the characteristics of the geothermal system in Wairakei. Taylor and Veronis [11] used a Hele–Shaw cell to study double-diffusive fingering. They found that the horizontal scale of the fingers is small in comparison to the plate spacing, and the convection cell breaks down as a model for groundwater fingers. An experimental investigation of fingering growth in two fluid layers of different densities saturating a porous medium was carried out by Imhoff and Green [12]. In their observations, they found that double-diffusive fingering convection can form in a saturated porous medium. By measuring the solute flux, they concluded that the fingering transport rate can be two orders of magnitude larger than that associated with the molecular diffusion in a motionless fluid. The width of the finger grew from about 0.3 cm at the sharp interface when the fingers were short to about 1.0 cm near the bottom when the fingers were long.

In this paper, we consider the double-diffusive fingering convection in a horizontal porous layer. The flow is assumed to be two-dimensional and periodic in the horizontal direction. The Darcy equation including Brinkman and Forchheimer terms is used for the momentum equation. To solve the equations and corresponding initial and boundary conditions, a Galerkin method is applied in the horizontal direction, and a hybrid finite difference method is used in the vertical direction. The hybrid method performs

time-differencing using the implicit scheme of Crank–Nicolson for the diffusion terms and the explicit Adams–Bashforth scheme for the nonlinear terms. This numerical algorithm is of second-order accurate in both time and space.

The developed computer code is first verified by the results of thermal convection case obtained by Combarnous and Bories [13], Georgiadis and Catton [14], and Chen and Chen [3]. Then the algorithm is applied to the salt-finger case. Lacking information about finite amplitude motion of fingering convection in a porous medium, we proceed with a series of computations by considering several selected thermal Rayleigh numbers within $1 \leqslant R_T \leqslant 50$, and increasing R_S stepwise to supercritical values.

2. GOVERNING EQUATIONS

We consider a horizontal porous layer of thickness h bounded with rigid boundaries at top and bottom. On the top boundary, the temperature and salinity are maintained constant and higher than those on the bottom. A Cartesian coordinate system is chosen with the origin at the bottom and the z-axis vertically upward. The continuity, momentum, energy, and solute equations are, respectively,

$$\nabla \cdot \mathbf{u} = 0 \tag{1}$$

$$\rho_r\left[\frac{1}{\phi}\frac{\partial \mathbf{u}}{\partial t} + \frac{B}{K}|\mathbf{u}|\mathbf{u}\right] = -\nabla P - \frac{\mu}{K}\mathbf{u}$$

$$-\rho_r g[1-\gamma(T-T_r)+\beta(S-S_r)]\mathbf{k} + \mu\nabla^2\frac{\mathbf{u}}{\phi} \tag{2}$$

$$G\frac{\partial T}{\partial t} + \mathbf{u}\cdot\nabla T = \kappa_T\nabla^2 T \tag{3}$$

$$\phi\frac{\partial S}{\partial t} + \mathbf{u}\cdot\nabla S = \kappa_S\nabla^2 S, \tag{4}$$

where ρ_r denotes the density of the fluid at reference temperature T_r, which is chosen to be T_h, the temperature of the top boundary. In above equations, the Boussinesq approximation has been applied and γ and β are defined as

$$\gamma = -\frac{1}{\rho_r}\left[\frac{\partial \rho}{\partial T}\right]_{P,S}, \quad \beta = \frac{1}{\rho_r}\left[\frac{\partial \rho}{\partial S}\right]_{P,T}, \tag{5}$$

and the coefficient G in (3) is the ratio of porous medium heat capacity to fluid heat capacity $(\rho_r C_p)_m/(\rho_r C_p)_f$. The use of Brinkman terms, as discussed by Nield [15], is important when the porosity is large. For a porous medium in which the solid phase consists of glass beads, K is obtained from the Kozeny–Carmen relation [13],

$$K = \frac{d^2}{150}\frac{\phi^3}{(1-\phi)^2}, \tag{6}$$

in which d is the diameter of the glass beads which constitute the porous medium. The thermal diffusivity of the porous medium, κ_T, is calculated from [13]

$$\kappa_T = \phi\kappa_f + (1-\phi)\kappa_g, \tag{7}$$

where κ_g is the thermal diffusivity of the glass, which is defined as the thermal conductivity of the glass divided by the specific heat capacity of the fluid. The solute diffusivity κ_S can be chosen to be 4.06×10^{-6} cm^2 s^{-1} (note that it is not necessary to explicitly use this dimensional value in subsequent computations), which is relevant to a porous medium consisting of 3 mm diameter glass beads immersed into a low concentration solution [9].

It has been realized that the inclusion of inertial effects by adding $\mathbf{u}\cdot\nabla\mathbf{u}$ cannot be correct. Beck [16] pointed out that this term vanishes identically if the flow is unidirectional and hence cannot represent the known effect (increase in drag) in that case. For many naturally occurring porous media, Nield and Joseph [17] showed that $|\mathbf{u}|\mathbf{u}$ is the appropriate inertia term in the momentum equation. This is a modification of an equation associated with the names of Dupuit and Forchheimer. The effect of inertia is a drag term in the momentum equation. The form drag constant B is independent of the viscosity and the other properties of the fluid but is dependent on the geometry of the medium. It can be expressed as [14]

$$B = \frac{1.75d}{150(1-\phi)}. \tag{8}$$

Experimental support for this form of the quadratic drag is described by Ward [18], while the many experimental results summarized by MacDonald *et al.* [19] are consistent with this form.

The boundary conditions at the top and bottom boundaries are non-slip, constant temperatures and salinities:

$$\mathbf{u} = 0, \quad T = T_h, \quad S = S_h \quad \text{at} \quad z = h, \tag{9}$$

$$\mathbf{u} = 0, \quad T = T_l, \quad S = S_l \quad \text{at} \quad z = 0. \tag{10}$$

To render the equations nondimensional, the depth of the layer h is chosen as the characteristic length, h^2/κ_T as time, $Pr\, v^2/h^2$ as pressure, v/h as velocity, $(T_h-T_l)v/\kappa_T$ as temperature, and $(S_h-S_l)v/\kappa_S$ as salinity, where v is kinematic viscosity. After nondimensionalizing and using the same notation for nondimensional quantities, the governing equations become

$$\nabla \cdot \mathbf{u} = 0 \tag{11}$$

$$\frac{1}{\phi\, Pr}\frac{\partial \mathbf{u}}{\partial t} + \frac{hB}{K}|\mathbf{u}|\mathbf{u} = -\nabla P + \frac{1}{\phi}\nabla^2\mathbf{u}$$

$$-\frac{1}{Da}\mathbf{u} + \frac{1}{Da}(R_T T - R_S S)\mathbf{k} \tag{12}$$

$$G\frac{\partial T}{\partial t}+Pr\,\mathbf{u}\cdot\nabla T=\nabla^2 T \tag{13}$$

$$\frac{\phi}{Le}\frac{\partial S}{\partial t}+Sc\,\mathbf{u}\cdot\nabla S=\nabla^2 S. \tag{14}$$

The nondimensional boundary conditions are

$$\mathbf{u}=0,\quad T=\frac{1}{Pr},\quad S=\frac{1}{Sc},\quad \text{at}\quad z=1, \tag{15}$$

$$\mathbf{u}=0,\quad T=0,\quad S=0,\quad \text{at}\quad z=0. \tag{16}$$

The important dimensionless parameters are the thermal Rayleigh number $R_T=g\gamma(T_h-T_l)hK/\nu\kappa_T$, solute Rayleigh number $R_S=g\beta(S_h-S_l)hK/\nu\kappa_S$, Prandtl number $Pr=\nu/\kappa_T$, Lewis number $Le=\kappa_S/\kappa_T$, Schmidt number $Sc=\nu/\kappa_S$, and Darcy number $Da=K/h^2$. Since equations (11)–(16) constitute an initial boundary value problem, an initial condition is needed. The computations are started from the quiescent basic state with linear vertical distributions of temperature and salinity plus a small vertically-sinusoidal perturbation in salinity of maximum amplitude $10^{-4}/Sc$.

3. NUMERICAL METHOD

The finite difference method and spectral method are two powerful methods to solve systems of partial differential equations (PDEs) arising from convection–diffusion problems. The latter is especially widely used in natural convection problems because relatively few degrees of freedom are needed to simulate a smooth function. In that case, both the computational storage and execution time could be reduced considerably. On the other hand, the advantage of a finite difference method is that the formulation for most kinds of boundary conditions is easy and banded rather than full matrices are obtained.

In this paper a mixed finite difference and Galerkin method is used to study the doubly-diffusive fingering convection in a 2-D horizontal porous layer. This method combining the advantages of both finite difference and Galerkin methods was first developed by Rogers and Beard [20] for axisymmetric Taylor–Couette flow. Later Meyer-Spache and Keller [21] successfully applied this method to detect the first branch of Taylor vortex solution bifurcating from Couette flow for both a wide and a narrow gap. McDonough [22] and Georgiadis and Catton [14] applied the same scheme to Rayleigh–Bénard convection in a horizontal fluid layer and a porous layer, respectively. Recently, Buell [23] extended this scheme to obtain three-dimensional solutions of natural convection in a horizontal fluid layer.

The basic idea of the 'mixed' method is to use the Galerkin method in the direction(s) where it is most convenient or efficient, and to use finite differencing in the other direction(s). Thus, the dependent variables are expanded in Fourier series in the direction(s) in which the solution is periodic. A system of PDEs containing derivatives with respect to time and the remaining spatial coordinate(s) is obtained. To deal with the nonlinear terms in these PDEs, Meyer-Spache and Keller [21] used a full Newton's method, while McDonough [22] performed a modal decoupling. Both methods require tedious iterations and initial guesses, or some *ad hoc* damping factors, whereas the modal decoupling significantly reduces arithmetic per iteration. To avoid these difficulties, we employ the Adams–Bashforth explicit scheme to deal with nonlinear terms and use the Crank–Nicolson scheme for the remaining terms. This hybrid implicit/explicit method is computationally efficient because the nonlinear terms are handled explicitly and, thus, iteration is avoided. In addition, the severe time step restriction characteristic of the explicit method is relaxed by advancing the diffusion terms implicitly (Crank–Nicolson).

The details of the mixed scheme applying to the current problem are described in the rest of this section. It is assumed that the flow exhibits a horizontal periodicity. Truncated Fourier series which are formed in the functional space spanned by an orthonormal basis are utilized to represent the solution [14]:

$$\begin{aligned}
v(y,z,t) &= 0+\sum_{k=1}^{N} V_k(z,t)\sin\alpha_k y\\
w(y,z,t) &= 0+\sum_{k=1}^{N} W_k(z,t)\cos\alpha_k y\\
T(y,z,t) &= T_0(z,t)+\sum_{k=1}^{N} T_k(z,t)\cos\alpha_k y\\
S(y,z,t) &= S_0(z,t)+\sum_{k=1}^{N} S_k(z,t)\cos\alpha_k y\\
P(y,z,t) &= P_0(z,t)+\sum_{k=1}^{N} P_k(z,t)\cos\alpha_k y\\
|\mathbf{u}|(y,z,t) &= Q_0(z,t)+\sum_{k=1}^{N} Q_k(z,t)\cos\alpha_k y,
\end{aligned} \tag{17}$$

where $\alpha_k=k\alpha$ with $k=1,2,3,\ldots,N$, and α is the nondimensional wavenumber found in the linear stability analysis [24] to be π.

Rabinowitz [25] proved the existence of small amplitude steady solutions of the Rayleigh–Bénard problem, which could be represented by the expansions in (17) with both $S=0$ and $Q=0$. McDonough [22] used equations (17) with $S=Q=0$ to compute steady supercritical thermal convection. The expansion of (17) has also been used by Georgiadis and Catton [14] to compute steady supercritical convection in a porous layer. By numerous numerical tests, McDonough [22] and Buell [23] have studied the convergence rates and the absolute accuracy of the technique. McDonough proved via computed results that the Fourier representation (17) converges uniformly and absolutely when the Rayleigh number is less than

the second critical value, which is about 11 times the first critical value [26]. He also showed that at medium Rayleigh number case the convergence appears to be nearly exponential.

After eliminating the pressure in (12) by taking the curl, we substitute (17) into the resulting equations, take Galerkin inner products in the y-direction and obtain a system of PDEs:

$$\left[\frac{1}{\phi\, Pr}\frac{\partial}{\partial t}+\frac{1}{Da}-\frac{1}{\phi}(\mathrm{D}^2-\alpha_k^2)\right](\mathrm{D}^2-\alpha_k^2)W_k = \frac{Bh}{K}F_{1,k}-F_{2,k} \quad (18)$$

$$\left[G\frac{\partial}{\partial t}-(\mathrm{D}^2-\alpha_k^2)\right]T_k = -Pr\,F_{3,k} \quad (19)$$

$$\left[G\frac{\partial}{\partial t}-\mathrm{D}^2\right]T_0 = -\frac{Pr}{2}\sum_{j=1}^{N}\mathrm{D}(W_jT_j) \quad (20)$$

$$\left[\frac{\phi}{Le}\frac{\partial}{\partial t}-(\mathrm{D}^2-\alpha_k^2)\right]S_k = -Sc\,F_{4,k} \quad (21)$$

$$\left[\frac{\phi}{Le}\frac{\partial}{\partial t}-\mathrm{D}^2\right]S_0 = -\frac{Sc}{2}\sum_{j=1}^{N}\mathrm{D}(W_jS_j). \quad (22)$$

The boundary conditions can be written as

$$T_0=\frac{1}{Pr},\quad S_0=\frac{1}{Sc},\quad T_k=S_k=W_k=\mathrm{D}W_k=0,\quad \text{at}\quad z=1, \quad (23)$$

$$T_0=0,\quad S_0=0,\quad T_k=S_k=W_k=\mathrm{D}W_k=0,\quad \text{at}\quad z=0, \quad (24)$$

in which $F_{n,k}$, $n=1$ to 4, are represented as follows:

$$F_{1,k} = -Q_0(W_k''-\alpha_k^2W_k)-Q_0'W_k' + \sum_{i=1}^{N}\sum_{j=1}^{N}\left[\alpha_k^2I_2(k,i,j)W_iQ_j - \frac{\alpha_k}{\alpha_i}I_1(k,i,j)(W_i''Q_j+W_i'Q_j')\right] \quad (25)$$

$$F_{2,k} = \frac{\alpha_k^2}{Da}[R_TT_k-R_SS_k] \quad (26)$$

$$F_{3,k} = T_0'W_k+\sum_{i=1}^{N}\sum_{j=1}^{N}\left[\frac{\alpha_j}{\alpha_i}I_1(i,j,k)W_i'T_j + I_2(k,i,j)W_iT_j'\right] \quad (27)$$

$$F_{4,k} = S_0'W_k+\sum_{i=1}^{N}\sum_{j=1}^{N}\left[\frac{\alpha_j}{\alpha_i}I_1(i,j,k)W_i'S_j + I_2(k,i,j)W_iS_j'\right]. \quad (28)$$

Both D and $'$ in the above equations denote z-derivatives. The convolution products I_1 and I_2 are

$$I_1(k,i,j)=\frac{2\alpha}{\pi}\int_0^{\pi/\alpha}\sin\alpha_k y\sin\alpha_i y\cos\alpha_j y\,\mathrm{d}y = \begin{cases}0.5, & j=|k-i|\\ -0.5, & j=k+i\\ 0, & \text{others}\end{cases} \quad (29)$$

$$I_2(k,i,j)=\frac{2\alpha}{\pi}\int_0^{\pi/\alpha}\cos\alpha_k y\cos\alpha_i y\cos\alpha_j y\,\mathrm{d}y = \begin{cases}0.5, & j=|k-i|\\ 0.5, & j=k+i\\ 0, & \text{others}\end{cases}. \quad (30)$$

The scalars of quadratic Forchheimer term, i.e. $|\mathbf{u}|$, are evaluated first in the physical plane by the relation $|\mathbf{u}|=(v^2+w^2)^{1/2}$ and then transformed to the spectral plane to evaluate Q_k by using the discretized Fast Fourier Transform (FFT) at each time step.

For solving nonlinear convection–diffusion equations in one spatial dimension, Peyret and Taylor [27] suggested the Crank–Nicolson/Adams–Bashforth hybrid scheme when diffusion (viscosity or thermal diffusivity) is not too small. This hybrid implicit/explicit method is computationally efficient because the nonlinear terms are handled explicitly and, thus, iteration is avoided. In addition, the severe time step restriction characteristic of the explicit method is relaxed by advancing the diffusion terms implicity. To illustrate the computation procedures more clearly, we choose (19) as a typical example to discretize as follows:

$$G\frac{T_k^{n+1}-T_k^n}{\Delta t}-\tfrac{1}{2}[L_k^{n+1}T_k+L_k^nT_k] = -Pr\,[C_1F_{3,k}^n-C_2F_{3,k}^{n-1}], \quad (31)$$

where L_k^n is the differential operator $\mathrm{D}^2-\alpha_k^2$ at time step n. At $t=0$, let $C_1=1$ and $C_2=0$ so that the nonlinear terms are advanced initially by the forward Euler method. Thereafter, $C_1=1.5$ and $C_2=0.5$ are used in the right-hand side of (31) until the end of the computation. The spatial derivatives in the z-direction are approximated by standard central differences. This scheme is second-order accurate in space and time.

The initial conditions are quiescent basic state with linear vertical distributions of temperature and salinity and a sinusoidal salinity perturbation in the z-direction with maximum magnitude of $10^{-4}/Sc$. We also tried three other different types of small perturbations for some cases of $R_T=1$. They are sinusoidal perturbations with two and ten times the fixed initial wavenumber, and a random perturbation. The final steady states obtained for all four initial conditions are exactly the same, as characterized by the Nusselt number and the kinetic energy of the flow. Only the time to reach steady state depends on the initial conditions. For all subsequent calculations, the

sinusoidal perturbation with one complete wavelength is used.

The usual von Neumann stability analysis is not applicable to the current study because of the inherent nonlinearity in the governing equations. A complete analysis of stability of the system represented by equations (1)–(4) and their respective boundary conditions (9) and (10) would be an enormous task. However, from a numerical determination of the stable region in the parameter space, Pruett [28] found for this hybrid scheme that as the finite difference grid is refined, smaller time steps are required. In this study, the number of grid points and the corresponding time steps used were essentially determined by trial and error. In general, for cases with higher R_T and R_S, finer grid and smaller time steps are needed. Convergence of the Fourier series deteriorates with higher R_T and R_S. A detailed discussion of the convergence of the mixed scheme can be found in McDonough [22].

4. RESULTS AND DISCUSSION

Since we make no attempt to pursue a parametric study with regard to Pr and Le in this study, $Pr = 4.5$ and $Le = 0.3$, which is relevant to salt–sucrose solution, are considered in all the computations of this paper. The Schmidt number can be obtained by $Sc = Pr/Le = 15$. For the other parameters, we have $\phi = 0.389$, $Da = 0.89 \times 10^{-5}$, $d = 3$ mm, $h = 3$ cm, and $G = 0.69$ corresponding to a porous medium consisting of 3 mm diameter glass beads saturated by water.

4.1. *Comparison with previous results*

Before we use the developed computer code to calculate the double-diffusive fingering convection in the porous medium, we apply it for verification to thermal convection cases which were done by both computational and experimental methods. It is known that the fluid remains stationary when the R_T is below the first critical value $-R_T = 4\pi^2$ [29], where heat is transferred by conduction alone. Note that, according to the definition of R_T in this paper, the value of R_T is negative for thermal convection case, in which the porous layer is heated from below. Otherwise, for fingering convection case, both R_T and R_S are positive. Above this value of $-R_T$, steady convection prevails until a second critical value is reached when oscillatory motion first appears. Our computation yields a value for the first critical $-R_T$ between 39 and 40 and the second critical $-R_T$ between 390 and 400. Caltagirone [30] used a finite difference scheme for flow in a square cell and found that the value of the second critical $-R_T$ is 384 ± 5; whereas the value reported by both Schubert and Straus [31] and Kimura *et al.* [32] is between 380 and 400 and more precisely 390.7 by Steen and Aidun [33]. Our computation for $-R_T = 480$ shows that the Nusselt number oscillates with a period of 0.0069, which compares well with the value of 0.0073 obtained by Schubert and Straus [31] (using our time scale). The Nusselt number fluctuates between 5.54 and 5.92 in the current study and between 5.61 and 5.95 in the work of Schubert and Straus. The Nusselt number in this study is defined as [22]

$$Nu = -\frac{dT_0}{dz} \quad \text{at} \quad z = 1. \tag{32}$$

Further checks of the computer code were made for the steady-state cases, i.e. $-R_T$ is smaller than 380. The results, as shown in Table 1, are in very good agreement with those of earlier investigations. Notice that in this study various numbers of terms of the Galerkin series are used for different R_T cases. A detailed discussion of the influence of the number of terms can be found in Schubert and Straus [31]. It is known that as $-R_T$ is increased into the supercritical range, heat transfer is maximized with the cells of decreasing wavelength. We have computed the Nusselt number over a range of wavenumbers from 2 to 8 at $R_T = -200$. These results are compared with those obtained by Combarnous and Bories [13] and by Georgiadis and Catton [14]. As shown in Fig. 1, the agreement between our results and those of Georgiadis and Catton is quite good, and that our results are generally higher than those of Combarnous and Bories, but with a similar trend.

4.2. *Double-diffusive fingering convection in supercritical stage*

In the rest of this section, we consider the supercritical fingering convection in a porous medium. The horizontal porous layer is heated and salted from above in which the thermal gradient serves as a stabilizing factor and solute gradient as a destabilizing factor. In each of the following computations, a sta-

Table 1. Comparison of steady-state Nusselt numbers for various R_T obtained in this study with the results obtained by previous studies

$-R_T$	100	200	300	350	380
Caltagirone [30]	2.651	3.813	4.523	—	—
Schubert and Straus [31]	—	—	—	4.79	4.94
Combarnous and Bories [13] Fig. 43	2.6	3.8	4.4	—	—
Present study	2.62	3.84	4.59	4.89	5.03
(No. of terms)	(5)	(5)	(10)	(15)	(15)

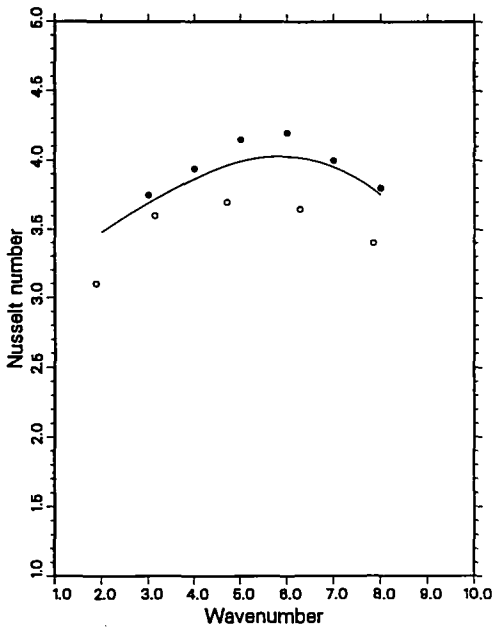

FIG. 1. Variation of the Nusselt number with wavenumber at $-R_T = 200$: —— present results; ● Georgiadis and Catton [14]; ○ Combarnous and Bories [13].

bilizing thermal gradient R_T and a destabilizing solute gradient R_S above the critical value are maintained. The value of R_S ranges from slightly above the critical to highly supercritical. The Nusselt and Sherwood numbers are the major measures of the strength of convection, and streamline patterns, isotherms and isoconcentration contours are used to study the transport phenomena. The Sherwood number is a dimensionless measure of the salt flux and has the same definition as the Nusselt number of (32) except T_0 is replaced by S_0.

As far as the authors are aware, there is no published literature that is devoted to the nonlinear fingering convection in the porous medium. Nield [24] determined the onset R_S theoretically for various boundary conditions. Straus [4] studied the finite amplitude fingering convection in a fluid layer and found that supercritical convective fingering is stable only when the wavelength is much smaller than that at the onset. Lacking further information about finite amplitude fingering convection in a porous medium, we pursue a computational study for R_S ranging from near the onset to highly supercritical. Two different values of R_T, 1 and 50, are considered in this section. For $R_T = 1$, we expect the convective motion to be similar to that of thermal convection; and a totally different phenomenon is anticipated for the case of $R_T = 50$, as discussed in Chen [34] for different geometrical configuration.

We examine the critical R_S by looking at the temporal evolution of the kinetic energy to determine if the initial disturbance grows or decays. A vertical sinusoidal perturbation of solute with an amplitude of $10^{-4}/Sc$ superimposed on a quiescent basic state with linear thermal and solutal gradients in the vertical direction is used as the initial condition. It turns out that the computed critical R_S is 41 for $R_T = 1$ and 90 for $R_T = 50$ compared with 40.5 and 89.5 of the linear stability analysis [24]. The agreement between nonlinear computation and linear theory is very good.

We then investigate the case of $R_T = 1$ by extending R_S from 1.5 to 11 times the critical. At a value of R_S between 10 and 11 times the critical, oscillatory convective motion sets in. For each value of R_S, extensive tests of convergence rate are conducted. The Nusselt numbers are the major measures for the convergence rate. A result with an error of less than 2%, which is attributed to the truncated terms, is regarded as the convergent solution. The error is evaluated on the basis of the results obtained by using the highest number of terms. From the experience of thermal convection cases, we are aware that the convergence rate of the Galerkin series is second order for the cases which attain steady solution. Nevertheless, more terms are needed to simulate the flow at higher Rayleigh numbers. For unsteady solutions, a much larger number of terms in the Galerkin series is necessary to obtain a convergent solution. This was also indicated by Schubert and Straus [31] as well as by Steen and Aidun [33].

Table 2 summarizes the results obtained for $R_T = 1$ with R_S varying from 1.5 to 10 times the critical. Different number of grid points and terms of Galerkin series are used to test the convergence of solution. It is found that, for $R_S = 5R_S^l$, the Nusselt and Sherwood numbers given by 5-term-50-point simulation are quite accurate compared with those from 12-term-50-point or 5-term-100-point simulations. For $R_S < 5R_S^l$, a smaller number of terms and grid points are needed to accurately simulate the solutions. In these cases, steady unicellular convection is obtained. When $R_S = 10R_S^l$, the results are more sensitive to the number of terms retained in the Galerkin series. From Table 2, with the number of grid points fixed at 50, one can see that oscillatory unicellular convection is obtained when only five terms are used. A steady state solution with tricellular convection is obtained using eight terms, and the Nusselt and Sherwood numbers differ considerably from the five-term results. When 12 terms are used, another oscillatory tricellular convection is again predicted. The convergent solution is not found until the number of terms increases to 16 and 20. The Nusselt numbers are almost the same using 16 terms and 20 terms, and the corresponding streamline patterns are essentially identical. To examine the finite difference discretization convergent rate, we use a 16-term-80-point discretization for $R_S = 10 \times R_S^l$ and find the Nusselt and Sherwood numbers differ by less than 1% from those obtained using a 16-term-50-point discretization. We summarize the steady-state convective patterns in terms of streamlines, isotherms and isoconcentration contours in Fig. 2 for $R_T = 1$.

Table 2. Nusselt and Sherwood numbers for various R_S and $R_T = 1$ with different number of terms used. (s1): steady state with single cell; (s3): steady state with triple cell; (o1): oscillatory state with single cell; (o3): oscillatory state with triple cell

No. of terms		5	8	12	16	20	5	5	16
No. of points		50	50	50	50	50	80	100	80
R_S/R_S^1									
1.5	*Nu*	1.096 (s1)	1.096 (s1)	—	—	—	1.092 (s1)	—	—
	Sh	1.746	1.746	—	—	—	1.740	—	—
3.0	*Nu*	1.415 (s1)	1.415 (s1)	—	—	—	1.409 (s1)	—	—
	Sh	2.946	2.946	—	—	—	2.937	—	—
5.0	*Nu*	1.809 (s1)	1.802 (s1)	1.797 (s1)	—	—	1.803 (s1)	1.801 (s1)	—
	Sh	3.870	3.837	3.821	—	—	3.834	3.822	—
10.0	*Nu*	2.900 (o1)	1.935 (s3)	2.100 (o3)	2.512 (s1)	2.512 (s1)	—	—	2.510 (s1)
	Sh	7.400	5.509	5.400	5.135	5.137	—	—	5.131

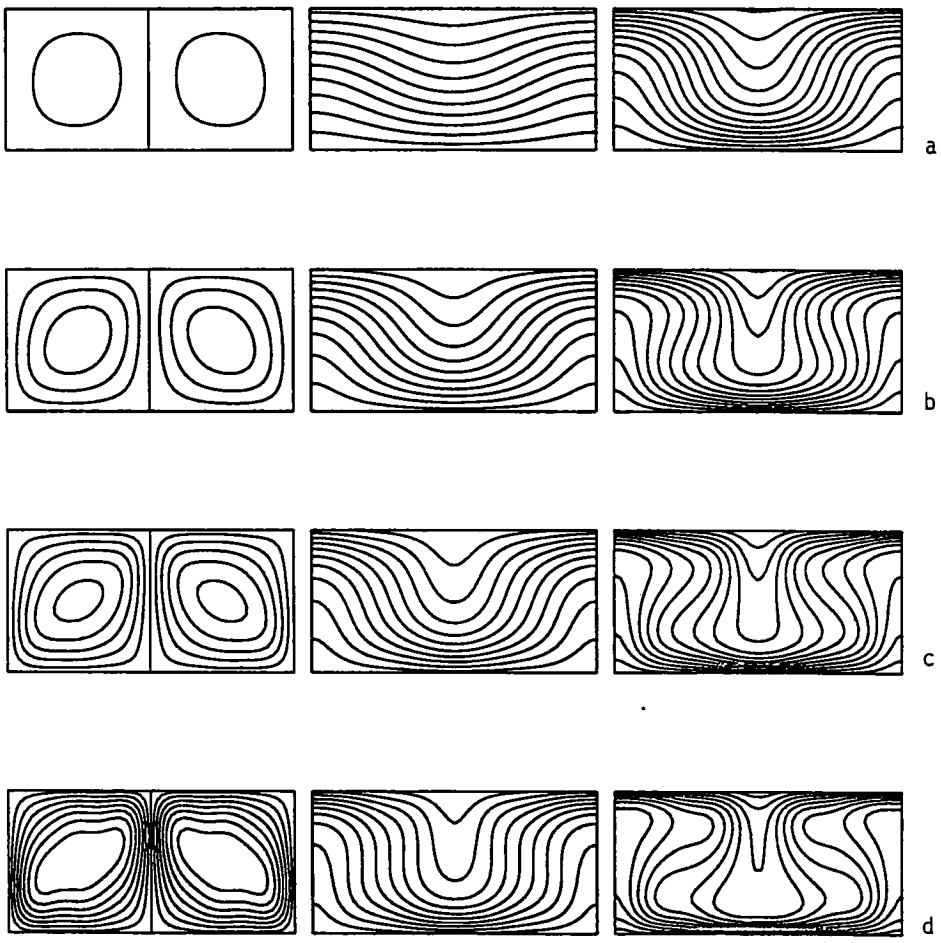

FIG. 2. Steady-state streamline patterns (left), isotherms (middle) and isoconcentration contours (right) for $R_T = 1$ with various R_S: (a) $R_S/R_S^1 = 1.5$; (b) $= 3$; (c) $= 5$; (d) $= 10$.

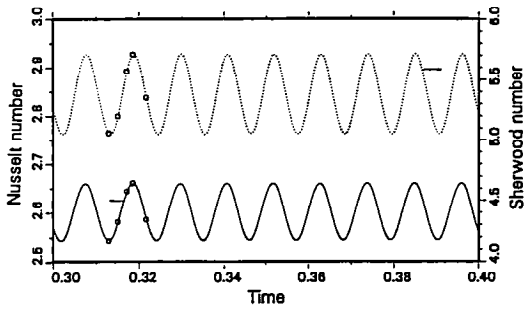

FIG. 3. Time evolution of Nusselt and Sherwood numbers of $R_T = 1$ and $R_S/R_S^1 = 11$.

In the thermal convection case, $-R_T = 390.7$ is the critical value for the onset of oscillatory motion; the so-called secondary onset. For $-R_T$ larger than the secondary onset, the flow becomes oscillatory with constant period and amplitude. In the fingering convection case of $R_T = 1$, we anticipate the secondary onset of R_S^2 will lie close to that of thermal convection. Accordingly, we compute the case of $R_S = 11R_S^1$ and find that the convection turns out to be oscillatory. The period is 0.011 and the Nusselt number oscillates between 2.01 and 3.23, and Sherwood number between 5.04 and 5.72. As can be seen in Fig. 3, the oscillation is regular and stable. In this computation, 30-term-50-point discretization is necessary to accurately simulate the oscillatory motion. A further computation using 30-term-80-point was conducted and resulted in a solution which differs from those of 30-term-50-point by less than 2% in the Nusselt and Sherwood numbers.

Higher values of secondary onset R_S^2 (between 405 and 445.5) of the fingering convection than those of the thermal convection are not surprising because in fingering convection, the temperature gradient, viscous dissipation, and thermal conduction are all stabilizing, in contrast to the thermal convection case in which only viscous dissipation and thermal conduction are stabilizing. It is evident that the temperature gradient makes a significant contribution in stabilizing the flow. By observing the streamline patterns and corresponding isotherms and isoconcentration contours during an oscillatory period, as shown in Fig. 4, we find that the flow is unicellular and speeds up and slows down during the cycle, and the convection pattern changes very little during a cycle.

The case of $R_T = 50$ is examined next. We increase R_S from 1.5 to 5 times the critical, at which value an oscillatory convection is found. Table 3 summarizes the results for $R_T = 50$. Convergence testing was done by increasing the number of terms in the Galerkin series. The number of grid points of the finite difference scheme is fixed at 50 since the experience gained in the $R_T = 1$ case shows that use of 50 points gives a solution within a reasonable error, i.e. less than 2% in Nusselt and Sherwood numbers; also the flow pattern is not affected by the resolution of the vertical discretization.

For $R_S = 1.5R_S^1$, five terms are enough to obtain a convergent solution, in which steady unicellular convection occurs. Increasing R_S to three times the critical, a five-term horizontal discretization results in an oscillatory unicellular convection. After adding three more terms in the series, a unicellular steady state is found and the Nusselt and Sherwood numbers are found to be in good agreement with those obtained using 12 terms. The number of terms again becomes more important for higher Rayleigh number. For $R_S = 4R_S^1$, a convergent solution is not available until 12 terms are used. The differences in Nusselt and Sherwood numbers between those obtained by 12 and 16 terms are negligible. Steady unicellular convection is found in this case. The streamline patterns and the corresponding isotherms and isoconcentration contours are shown in Fig. 5.

An oscillatory phenomenon is observed when R_S increases to five times the critical value. Twenty-five terms are necessary to simulate the oscillatory fingering convective flow in this case. A comparison (not shown) was made between the periods and amplitudes obtained using 30 terms and 25 terms to assure that the solution converged. Figure 6 illustrates the evolution of Nusselt and Sherwood numbers with time and shows that the oscillation is multipeaked periodic. The period is almost exactly twice that which occurs at $R_T = 1$ and $R_S = 11R_S^1$. To gain physical insight during the oscillations, the streamlines, isotherms and isoconcentration contours between $t = 0.42$ and $t = 0.44$ are presented in Fig. 7. One can see that the core of the convection cell moves back and forth along the diagonal of the square and the convective flow pattern keeps a similar profile.

4.3. *Identification of stability boundaries*

In the last section, we found that the steady fingering convection becomes an unsteady motion in $10 < R_S/R_S^1 < 11$ for $R_T = 1$ and in $4 < R_S/R_S^1 < 5$ for $R_T = 50$. In order to more precisely identify the R_S^2, at which an unsteady convective flow bifurcates from the steady solution, we compute several cases with $R_S > R_S^2$ for four selected $R_T = 1$, 15, 30, and 50. The value of R_S^2 is determined by intersecting the curves of steady convection and unsteady convection (see Fig. 8). For $R_T = 1$, for instance, we compute the Sherwood (also the Nusselt) number of four cases of $R_S/R_S^1 = 1.5$, 3, 5, and 10 for steady convection. Together with the onset point at $R_S = R_S^1$, a smooth curve of Sherwood number versus R_S consisting of five points is made. We also compute the Sherwood number for $R_S/R_S^1 = 11$, 12, and 13, in which the convective motion is periodic. The mean value of Sherwood number in a period is taken for determining a point of the curve of periodic convection. The curve connecting these three points has a different slope to that of steady convection. By extending both curves

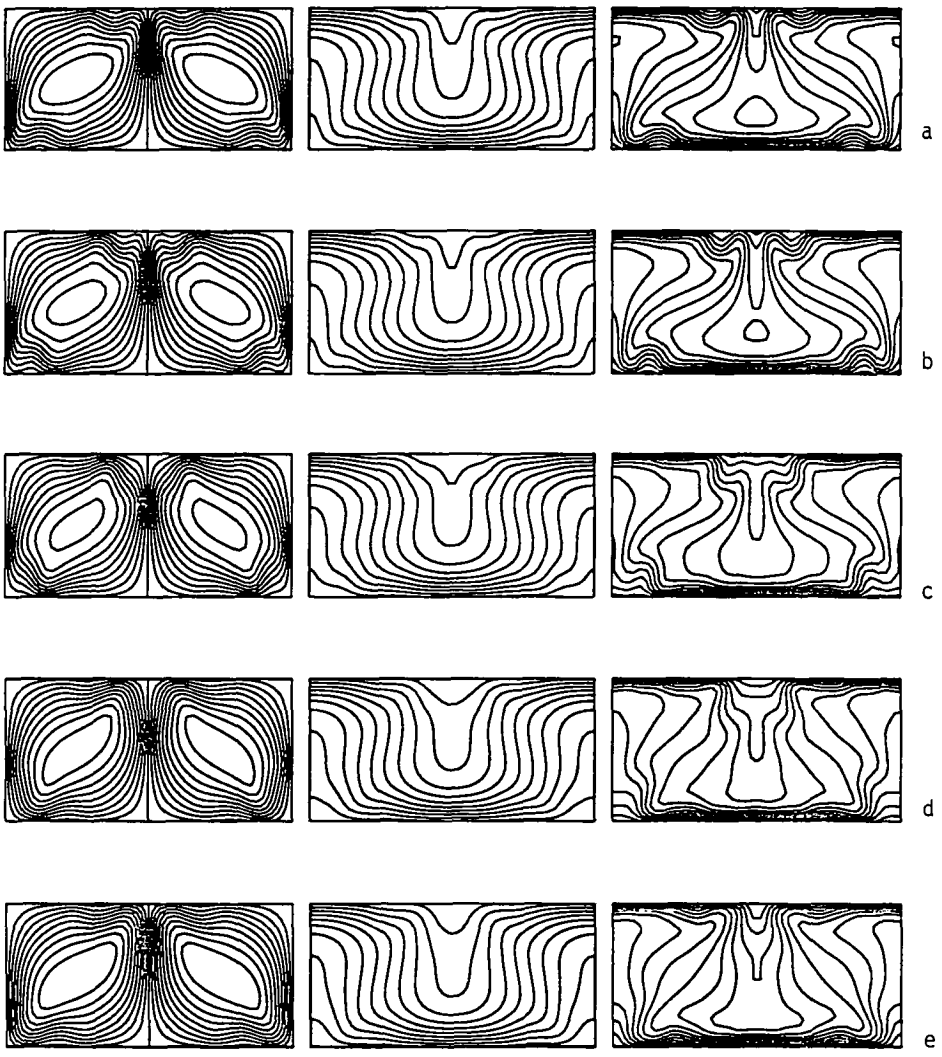

FIG. 4. Streamline patterns (left), isotherms (middle) and isoconcentration contours (right) corresponding to times indicated in Fig. 3: (a) $t = 0.313$; (b) $t = 0.315$; (c) $t = 0.317$; (d) $t = 0.319$; (e) $t = 0.322$.

with dashed curves and seeking the intersection point, the R_S^2 is thus approximately determined to be 440. Using the same method of intersecting the extending curves, the R_S^2 and R_S^3, at which the convection bifurcates from periodic to unsteady (or multipeaked-periodic), for $R_T = 50$ are approximately determined to be 405 and 440, respectively. The curve of steady convection consists of four points at $R_S/R_S^1 = 1$, 1.3, 3, and 4 and that of periodic convection is composed of three points at $R_S = 410$, 420, and 430. For the curve of unsteady convection, we consider three cases of $R_S/R_S^1 = 5$, 6, and 7, in which unsteady convection prevails. We use a vertical bar to represent the range of fluctuation of Sherwood number for each case. The curve of unsteady convection is made by connecting the central points of these three bars.

For $R_T = 15$ and 30, the values of R_S^2 and R_S^3 are determined by the same method. With these computed critical Rayleigh numbers, the boundaries between different types of convective motion can be identified (Fig. 9). Figure 9 illustrates four different regions: a quiescent region where the fluid is motionless, a steady convection region where the convective motion is steady, a periodic convection region where the convective motion changes periodically, and an unsteady convection region where the convection either is multipeaked-periodic when R_S is close to R_S^3 or is arbitrarily unsteady, in which the Nusselt or Sherwood number fluctuates in a finite range, when R_S is much larger than R_S^3. The boundary between quiescent and steady convection region is determined by the relation [24]

$$R_S = R_T + 4\pi^2. \tag{33}$$

The boundary dividing regions of steady and periodic convection is represented by the curve consisting of five points. The regions of unsteady and periodic con-

Table 3. Nusselt and Sherwood numbers for various R_S and $R_T = 50$ with different number of terms used. (s1): steady state with single cell; (s3): steady state with triple cell; (o1): oscillatory state with single cell; (o3): oscillatory state with triple cell

No. of terms R_S/R_S^1		5	8	12	16	20	25
1.5	*Nu*	1.114 (s1)	1.114 (s1)	—	—	—	—
	Sh	1.862	1.861	—	—	—	—
3.0	*Nu*	1.500 (o1)	1.532 (s1)	1.527 (s1)	—	—	—
	Sh	3.401	3.325	3.319	—	—	—
4.0	*Nu*	2.000 (o1)	1.613 (s3)	1.808 (s1)	1.807 (s1)	—	—
	Sh	5.000	4.640	3.944	3.942	—	—
5.0	*Nu*	—	1.700 (o3)	1.951 (s3)	2.200 (o1)	2.300 (o1)	—
	Sh	—	4.700	5.859	5.100	5.200	—

vection are separated by the curve consisting of three calculated points and one point of $R_T = 0$, the thermal convection case. This was determined by Kimura *et al.* [35] to be the point at which the thermal convection changes from periodic motion to an unsteady chaotic state in the range $850 < -R_T < 1000$, and 950 is chosen in Fig. 9. In fact, the boundaries are estimated with some errors, which generally lie within ± 20 of R_S.

The value of R_S^3 for $R_T = 1$ cannot be obtained by the current scheme because of the large number of terms of Galerkin series needed as well as the severe limit of time step. We tabulate in Table 4 the periods corresponding to the onset of periodic motion at R_S^2

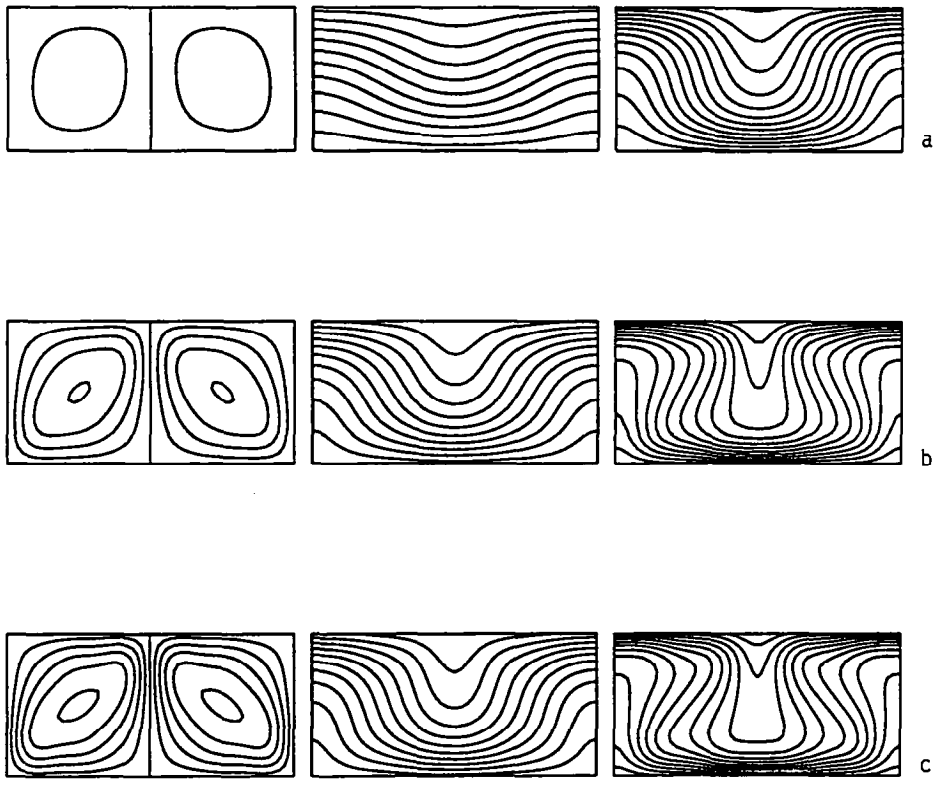

FIG. 5. Steady-state streamline patterns (left), isotherms (middle) and isoconcentration contours (right) for $R_T = 50$ with various R_S: (a) $R_S/R_S^1 = 1.5$; (b) $= 3$; (c) $= 4$.

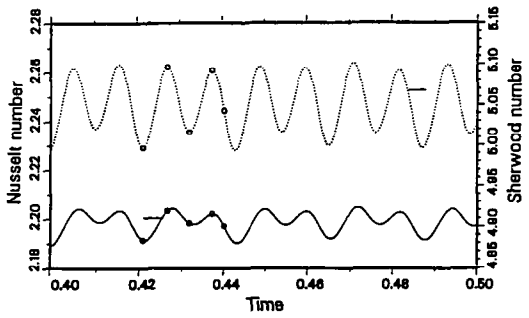

FIG. 6. Time evolution of Nusselt and Sherwood numbers of $R_T = 50$ and $R_S/R_S^1 = 5$.

for various R_T considered. As one can see, the period decreases with increasing R_S^2, but not much. For $R_T = 50$, the period of $R_S = 430$ is about the same with that of $R_T = 1$ and $R_S = 445.5$. As R_S increases to 452.5 for $R_T = 50$, the convective motion becomes multipeaked-periodic with a period being about twice of that of $R_S = 430$. Note that for $15 \leqslant R_T \leqslant 50$, the periodic motion is of single period. For R_T close to zero, according to Kimura *et al.* [35], the periodic motion may be of single or double period. For unsteady convection, the fluid motion is either multipeaked-periodic or arbitrarily unsteady.

4.4. *Comments on the numerical scheme*

A few comments on the mixed finite difference–Galerkin scheme used here are made in the following. From Tables 2 and 3 one can find that the Fourier

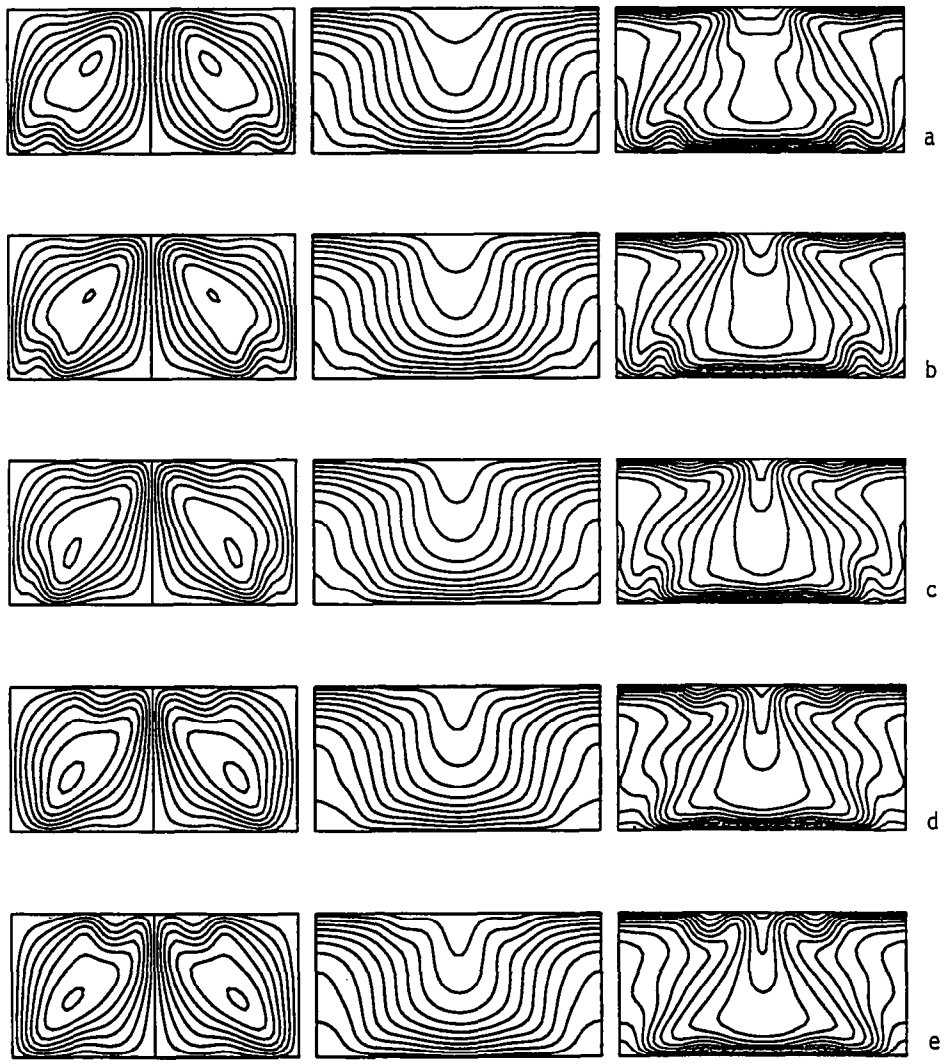

FIG. 7. Streamline patterns (left), isotherms (middle) and isoconcentration contours (right) corresponding to times indicated in Fig. 6: (a) $t = 0.421$; (b) $t = 0.427$; (c) $t = 0.432$; (d) $t = 0.437$; (e) $t = 0.441$.

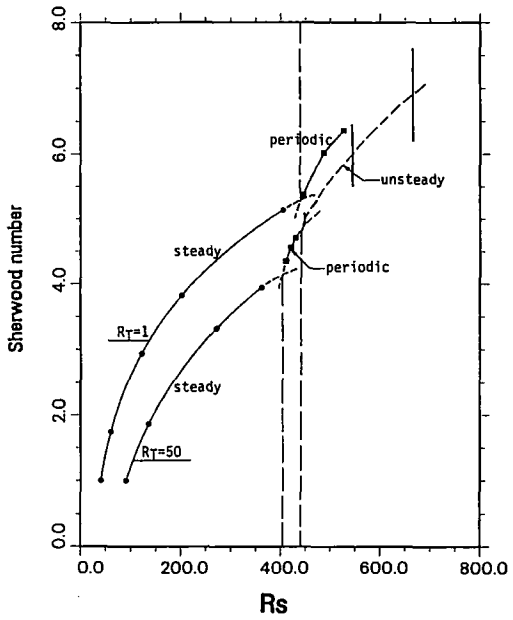

FIG. 8. Sherwood numbers for various R_S and $R_T = 1$ and 50 at different state of convective flow.

series converges faster than the series $\Sigma_{N=1}^{\infty}(1/N^2)$, where N is the number of terms of Galerkin series, when the solution is steady. As R_S increases beyond R_S^2, according to the discussion of McDonough [22] and of this study, the convergent rate becomes much slower. We tabulate the corresponding computational data for the computation done in Section 4.3 in Table 4, from which one can see the number of terms of Galerkin series is dramatically larger than that needed for a steady state. We also show in Fig. 10 the CRAY XMP/48 CPU time required for every thousand time steps when the number of grid points and terms increase. The case we use to examine CPU time is $R_T = 1$ and $R_S = 1.5R_S^1$. It is found that the CPU time increases exponentially with the number of terms while increasing linearly with the number of grid points. The results shown in Sections 4.1 and 4.2 were obtained by using the CRAY XMP/48 at University of California at San Diego. The results of Section 4.3 were obtained by using Convex C-1 at National Taiwan University, whose computational speed is much slower than that of CRAY XMP/48. To run a case using 40 terms and 50 points for 1000 time steps, for example, with the time sharing system setup in the operational system of Convex C-1, three days are necessary to run through a case. Usually, for obtaining an unsteady solution, more than 2000 time steps are required. In conclusion, the current scheme is quite efficient for the steady state while is relatively time-consuming if the solution is unsteady.

Table 4. Periods and corresponding computational data used for each case of various R_T and R_S

R_T	R_S	No. of terms	Time step	Period
1	445.5	30	0.0001	0.011
	486.5	30	0.0001	0.0084
	526.5	35	0.00005	0.0071
15	530	30	0.0001	0.0098
	550	35	0.00005	0.0091
	600	35	0.00002	0.0074
	700	45	0.00001	—
30	480	25	0.0001	0.011
	500	25	0.0001	0.010
	600	35	0.00002	—
50	410	25	0.0001	0.013
	420	25	0.0001	0.013
	430	25	0.0001	0.011
	452.5	25	0.0001	—
	543	40	0.00001	—
	633.5	40	0.00001	—

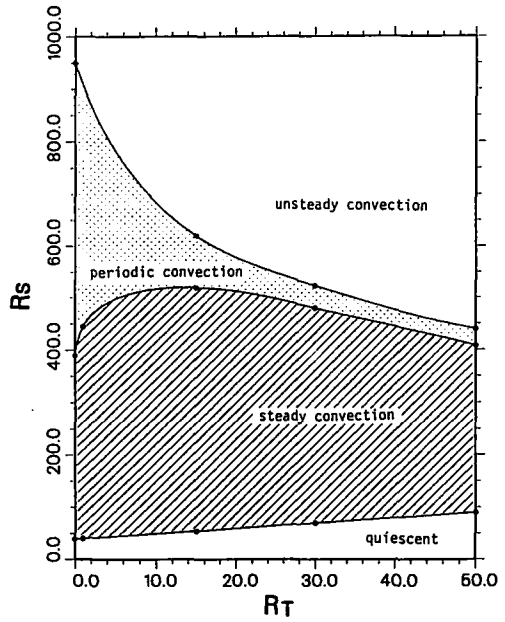

FIG. 9. Stability boundaries dividing regions of different convective flow.

5. SUMMARY

We have considered nonlinear two-dimensional double-diffusive fingering convection in a horizontal porous medium in which a horizontally-periodic condition is prescribed. A mixed Galerkin–finite difference method is developed to numerically solve the initial boundary value problem, which is governed by Darcy's law, including Brinkman and Forchheimer terms to account for viscous and inertia effects, respectively, and the associated energy and mass transfer equations. The developed computer code was first used to compute the thermal convection case and the results were in good agreement with existing results. In the fingering convection case, we considered four selected values of $R_T = 1$, 15, 30, and 50. For each

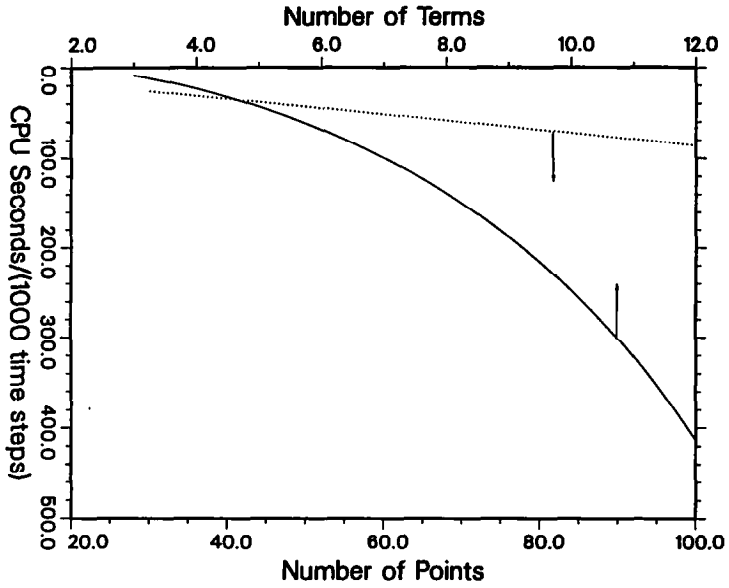

FIG. 10. CPU time required for various numbers of terms of Galerkin series and grid points of finite difference discretization.

case of R_T, three kinds of critical R_S are determined; they are R_S^1 the critical value for the onset of steady fingering convection, R_S^2 for the transition from steady convection to periodic convection, and R_S^3 for the transition from periodic convection to unsteady convection. With these critical R_S and corresponding R_T, the stability boundaries dividing the regions of different kinds of fluid motion are identified in a R_T–R_S plane. The mixed Galerkin–finite difference scheme used in this study is found to be quite efficient when the convective motion is steady while is relatively time consuming for unsteady or periodic convection since a large number of terms in the Galerkin series is required to reach a convergent solution.

Acknowledgement—The authors like to acknowledge the financial support of NSF Grant MSM-87-02732 and NASA Grant NAG-3-723. The computing service and computing time provided by the San Diego Supercomputer Center (CRAY XMP/48) are gratefully acknowledged.

REFERENCES

1. J. S. Turner, Multicomponent convection, *Ann. Rev. Fluid Mech.* **17,** 11–44 (1985).
2. M. E. Glicksman, S. R. Coriell and G. B. McFadden, Interaction of flows with crystal–melt interfaces, *Ann. Rev. Fluid Mech.* **18,** 307–335 (1986).
3. F. Chen and C. F. Chen, Onset of finger convection in a horizontal porous layer underlying a fluid layer, *ASME Trans., J. Heat Transfer* **110,** 403–409 (1988).
4. J. M. Straus, Finite amplitude double diffusive convection, *J. Fluid Mech.* **56,** 353–374 (1972).
5. S. A. Piacsek and J. Toomre, Nonlinear evolution and structure of salt fingers. In *Marine Turbulence* (Edited by J. C. J. Nihous), pp. 193–219. Elsevier, New York (1980).
6. H. E. Huppert and D. R. Moore, Nonlinear double-diffusive convection, *J. Fluid Mech.* **78,** 821–854 (1976).
7. E. Knobloch, D. R. Moore, J. Toomre and N. D. Weiss, Transitions to chaos in two-dimensional double-diffusive convection, *J. Fluid Mech.* **166,** 409–448 (1986).
8. B. T. Murray, Experimental and numerical investigation of double-diffusive convection in a horizontal layer of porous medium, Ph.D. dissertation, University of Arizona, Tucson (1986).
9. B. T. Murray and C. F. Chen, Double-diffusive convection in a porous medium, *J. Fluid Mech.* **201,** 147–166 (1989).
10. R. W. Griffiths, Layered doubly-diffusive convection in porous media, *J. Fluid Mech.* **102,** 221–248 (1981).
11. J. Taylor and G. Veronis, Experiments on salt fingers in a Hele–Shaw cell, *Science* **231,** 39–41 (1986).
12. P. T. Imhoff and T. Green, Experimental investigation of double-diffusive groundwater fingers, *J. Fluid Mech.* **188,** 363–382 (1988).
13. M. A. Combarnous and S. A. Bories, Hydrothermal convection in saturated porous media, *Advances in Hydroscience* **10,** 231–307 (1975).
14. J. G. Georgiadis and I. Catton, Prandtl numbers effect on Benard convection in porous media, *ASME Trans., J. Heat Transfer* **108,** 284–290 (1986).
15. D. A. Nield, The boundary correction for the Rayleigh–Darcy problem: limitation of the Brinkman equation, *J. Fluid Mech.* **128,** 37–46 (1983).
16. J. L. Beck, Convection in a box of porous material saturated with fluid, *Physics Fluids* **15,** 1377–1383 (1972).
17. D. A. Nield and D. D. Joseph, Effect of quadratic drag on convection in a saturated porous medium, *Physics Fluids* **28,** 995–997 (1985).
18. J. C. Ward, Turbulent flow in porous media, *J. Hydraulics Div., ASCE* **90,** 1–13 (1964).
19. I. F. MacDonald, M. S. El-Sayed, K. Mow and F. A. L. Dullien, Flow through porous media—the Ergun equation revisited, *Ind. Engng Chem. Fund.* **18,** 199–208 (1979).
20. E. H. Rogers and D. W. Beard, A numerical study of wide gap Taylor vortices, *J. Comp. Phys.* **4,** 1–18 (1969).

21. R. Meyer-Spache and H. B. Keller, Computations of the axisymmetric flow between rotating cylinders, *J. Comp. Phys.* **35,** 100–109 (1980).
22. J. M. McDonough, The Rayleigh–Bénard problem on a horizontally unbounded domain: determination of the wavenumber of convection, Ph.D. dissertation, UCLA, Los Angeles (1980).
23. J. C. Buell, A mixed finite difference/Galerkin method for three-dimensional Rayleigh–Bénard convection, *J. Comp. Phys.* **75,** 54–72 (1988).
24. D. A. Nield, Onset of thermohaline convection in a porous medium, *Water Resources Research* **4,** 553–560 (1968).
25. P. H. Rabinowitz, Existence and nonuniqueness of rectangular solutions to the Benard problem, *Arch. Ration. Mech. Analysis* **29,** 32–57 (1968).
26. R. Krishnamurti, Some further studies on the transition to turbulent convection, *J. Fluid Mech.* **60,** 285–303 (1973).
27. R. Peyret and T. D. Taylor, *Computational Methods for Fluid Flow*. Springer, Berlin (1982).
28. C. D. Pruett, Numerical simulation of nonlinear waves in free shear layer, Ph.D. dissertation, University of Arizona, Tucson (1986).
29. E. R. Lapwook, Convection of a fluid in a porous medium, *Proc. Camb. Phil. Soc.* **44,** 508–521 (1948).
30. J. P. Caltagirone, Thermoconvection instabilities in a horizontal porous layer, *J. Fluid Mech.* **72,** 269–287 (1975).
31. G. Schubert and G. M. Straus, Transitions in time-dependent thermal convection in fluid-saturated porous media, *J. Fluid Mech.* **121,** 301–313 (1982).
32. S. Kimura, G. Schubert and J. M. Straus, Route to chaos in porous-medium thermal convection, *J. Fluid Mech.* **166,** 305–324 (1986).
33. P. H. Steen and C. K. Aidun, Time-periodic convection in porous media: transition mechanism, *J. Fluid Mech.* **196,** 263–290 (1988).
34. F. Chen, On the stability of salt-finger convection in superposed fluid and porous layers, *ASME Trans., J. Heat Transfer* **112,** 1088–1092 (1990).
35. S. Kimura, G. Schubert and J. M. Straus, Route to chaos in porous-medium thermal convection, *J. Fluid Mech.* **166,** 305–324 (1986).